Spherical Aperture-Coupled Antennas with Parasitic Element

Javad S. Meiguni [1], Manoochehr Kamyab [1], and Ahmad Hosseinbeig [1]

[1] Faculty of Electrical and Computer Engineering
K. N. Toosi University of Technology, PO Box 16315-1355, Tehran 1431714191, Iran
meiguni@ee.kntu.ac.ir, kamyab@eetd.kntu.ac.ir, hosseinbeig@ee.kntu.ac.ir

Abstract ─ Theory and experiment of spherical aperture-coupled antennas with parasitic elements are presented in this paper. Current distributions on slot and conformal patches are calculated using spatial domain electric and magnetic Dyadic Green's Functions (DGFs). Electromagnetic fields for such a structure have been calculated with the aid of linear Rao-Wilton-Glisson (RWG) triangular basis functions and by converting spherical DGFs to Cartesian DGFs. In order to validate the proposed method, a prototype of this antenna is fabricated and tested. The effect of parasitic element on antenna characteristics such as gain and radiation pattern is investigated. Good agreement between the results shows accuracy and high convergence speed of the presented method.

Index Terms - Dyadic Green's function, parasitic element, spherical aperture-coupled antennas, spherical to Cartesian transformation of DGFs.

I. INTRODUCTION

Aperture-coupled antennas have been investigated theoretically and experimentally over past decade. In such an antenna feed region is isolated from radiating region of the antenna due to the existence of ground plane. This property results in wide impedance matching and optimal array performance and shields the antenna elements from spurious radiation emitted by the feed line and RF devices [1-3].

Antennas mounted on multilayer spherical structures have been studied in recent years. Circular polarization can be achieved by proper design of these antennas which are suitable for satellite base stations and Line of Sight (LOS) applications [4-5]. There are several methods to analyze spherical antennas. Analysis methods based on Green's functions are more precise and faster [6-8]. In [9], a generalized method for the analysis of microstrip antennas placed on or embedded in multilayer hemispheres has been presented by using corresponding full-wave equivalent circuits. A hemispherical Dielectric Resonator Antenna (DRA) fed by a coaxial probe has been studied theoretically and experimentally in [10]. Both delta gap and magnetic frill source models have been considered to obtain the probe current from which the input impedance of the DRA has been calculated. Many investigations have been reported concerning DRAs located above slotted conducting plates [11-12]. The slot can be excited by a coaxial probe or through a microstrip line below the aperture. The existence of parasitic element improves impedance characteristics, directs antenna radiation patterns and reduces side lobes levels of patterns [13]. The use of a parasitic element in a DRA perturbs electromagnetic fields and excites two nearly degenerate orthogonal modes resulting in circular polarization [5].

In this paper, a multilayer spherical aperture-coupled antenna with a parasitic element is investigated. Due to the existence of spherical ground plane, the proposed antenna occupies less space in comparison with a DRA above a Perfect Electric Conductor (PEC) sheet. Current distribution on the narrow slot fed symmetrically by a coaxial probe is obtained by using mode-matching method and spatial domain Green's functions. Mutual couplings between slot and conformal antennas are calculated using scattering coefficients of magnetic DGFs of a multilayer sphere. A new approach is presented to convert spherical DGFs to Cartesian ones which is applied in calculation of electromagnetic fields inside and

Submitted On: July 7, 2012
Accepted On: Nov. 23, 2012

outside the antenna. The radiating elements are meshed with linear triangles. The effect of conformal patches on the slot is developed and the input impedance and radiation patterns of such an antenna are evaluated. A prototype is fabricated and tested and the measurement results are compared with those obtained from the proposed method.

II. THEORY

Figure 1 shows a spherical multilayer aperture-coupled antenna. Radiating elements may be of any arbitrary shape. Circular elements are preferred here due to their homogenous current distributions which result in lower side lobes levels in antenna radiation patterns. Each layer has permittivity and permeability of ε_i , μ_i, respectively. The conducting spherical core (layer 4) is modeled by $\varepsilon_4 \to \infty$, $\mu_4 \to 0$ in order for the propagation constant to be finite [14]. Full-wave analysis of this antenna is performed by using electric and magnetic DGFs of a four-layer sphere. The analysis based on DGFs and Method of Moments (MoM) has more calculation speed and accuracy in comparison with simulator packages. Simulator packages are highly dependent on meshing the structure, probe modeling and the size of radiation box. These limitations are not encountered in the presented analysis. Convergence speed of multilayer spherical DGFs is related to the radii of spheres and permittivities of layers. More spherical harmonic terms should be considered for greater radii and permittivities.

A. Analysis of Conformal Aperture-Coupled Antenna with Parasitic Element

Full-wave analysis of this antenna is performed by first investigating the effect of the rectangular slot by using the approach presented in [15]. Afterward, mutual couplings between the slot and conformal radiating elements are computed by using scattering DGFs of a four-layer sphere. The rectangular narrow slot can be analyzed using mode-matching method in spatial domain [15]. Based on the equivalence principle, magnetic current in the slot ($\mathbf{M}_s$) is modeled by a $2\mathbf{M}_s$ magnetic current over a whole sphere.

A delta gap source is used to model the excitation current. For a slot located between air and dielectric medium, as shown in Fig. 1, $k_e = \sqrt{(\varepsilon_r + 1)/2}\, k_0$ is the effective wave number of the slot. As this method is reported in details in [15], it will not be repeated here.

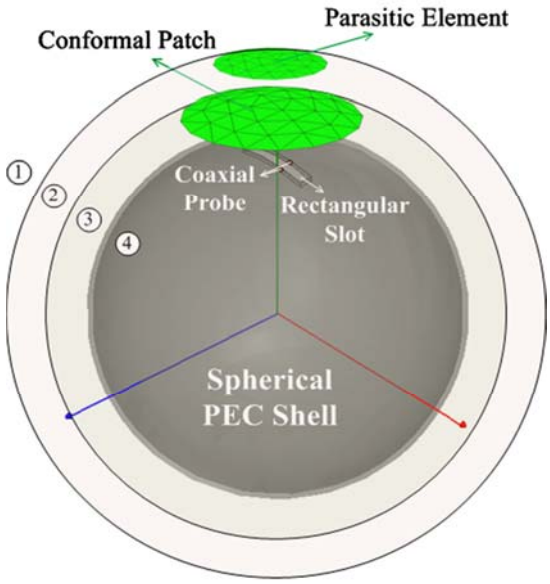

Fig. 1. Spherical aperture-coupled antenna with parasitic element.

A coaxial probe can be used to excite the slot. In this case, feed position affects the input impedance of the antenna. Regarding the input impedance diagram of the slot, the resonance frequency of the slot can be distinguished from those of the sphere due to high quality factor resonances of the sphere. If the slot is excited from its center, its second harmonic response does not affect the input impedance and subsequently the resonance frequencies of the sphere [15].

After calculating the magnetic current in the slot, magnetic fields ($\mathbf{H}$) on radiating elements are derived by using magnetic DGFs. The electric surface currents on these elements are computed from $\mathbf{J}_s = \mathbf{n} \times \mathbf{H}$, where $\mathbf{n}$ is the normal vector to the surface of the sphere. Magnetic field due to $\mathbf{M}_s$ in the slot is carried out by using the following expression:

$$\mathbf{H}(r,\theta,\varphi) = -j\omega\varepsilon_f \iint_{s'} \overline{\mathbf{G}}_M^{(fs)} \cdot \mathbf{M}_s(\mathbf{r}'(r',\theta',\varphi'))\, ds'. \quad (1)$$

$\mathbf{r}(r,\theta,\varphi)$ and $\mathbf{r}'(r',\theta',\varphi')$ refer to field and source vectors, respectively. The surfaces of patch antenna and parasitic element are meshed by linear triangles in order to calculate current distributions. Vector currents are assigned on common edges between plus and minus triangles based on RWG

method [16]. The centers of triangles are used to compute $\overline{\mathbf{G}}_M^{(fs)}$. Magnetic field of a conformal antenna can be calculated with good approximation by applying 3-point Gauss-Legendre integration. Equations of the required magnetic DGFs are presented in appendix1. The double summation in the spherical DGFs can be reduced to an expression with only a single summation by using the following relation [17]:

$$P_n(\cos\gamma)=\sum_{m=0}^{n}\left(2-\delta_m^0\right)\frac{(n-m)!}{(n+m)!} \times P_n^m(\cos\theta)\,P_n^m(\cos\theta')\cos\left(m(\varphi-\varphi')\right), \quad (2)$$

where $\cos\gamma=\cos\theta\cos\theta'+\sin\theta\sin\theta'\cos(\varphi-\varphi')$. This technique increases the convergence speed of DGFs. In the analysis of the studied antenna, the first 25 terms in the summation are considered regarding the size and dielectric constants of layers. Dimensions of the spherical aperture-coupled antenna with radiating elements are given in Table 1.

Table 1: Dimensions of the spherical aperture-coupled antenna with radiating elements

PEC sphere radius	50 mm
Layer 2 (ε_r=1) thickness	20 mm
Layer 3 (ε_r=2.33) thickness	0.8 mm
Rectangular slot	3 mm*20 mm
Conformal patch antenna	$0^\circ < \theta_{Patch} < 20.3^\circ$
Parasitic element	$0^\circ < \theta_{Parasitic} < 7^\circ$

The input impedance of the antenna is affected by the loading of conformal radiating elements above the slot. However, the fundamental excited mode in the slot is not changed (i.e. TE_{10} mode, assuming a narrow slot) and the direction of the electric field vector is transverse to the width of the slot. It can be shown that the parasitic element has negligible effect on the current distribution of conformal patch. Therefore, it is sufficient to take into account the loading effects of patch and parasitic element on the slot in the computation of the input impedance. In this case, electric field in the slot (layer 3) can be computed after calculating $\mathbf{J}_{s1}$ and $\mathbf{J}_{s2}$ which are current distributions on parasitic element and patch antenna, respectively. Then considering $\mathbf{E}^{(3)}$ as the electric field in the slot due to $\mathbf{J}_{s1}$ and $\mathbf{J}_{s2}$, the coupled magnetic current in the slot is calculated by using $\mathbf{M}_{1s}=-\mathbf{n}\times\mathbf{E}^{(3)}$, in which:

$$\mathbf{E}^{(3)}=-j\omega\mu_3\left(\begin{array}{l}\iint_{s'}\overline{\mathbf{G}}_E^{(31)}.\mathbf{J}_{s1}(\mathbf{r}')\,ds'+\\ \iint_{s'}\overline{\mathbf{G}}_E^{(32)}.\mathbf{J}_{s2}(\mathbf{r}')\,ds'\end{array}\right), \quad (3)$$

where $\overline{\mathbf{G}}_E^{(31)}$ and $\overline{\mathbf{G}}_E^{(32)}$ have been presented in [18].

B. Spherical to Cartesian Transformation of DGFs

In order to obtain electromagnetic field components, multiplication of DGFs and current element vector components is required in the same coordinates. If the conformal antenna surface is divided into curvilinear triangles as shown in Fig. 2 (a), θ and φ components of the current vector are considered which are in harmony with spherical components of DGFs [15]. However choosing curvilinear meshing in general can be complicated as compared with linear triangular meshing considered in this paper. As current vectors on common edges of linear meshes have Cartesian components, a new approach for dyad and vector multiplication is presented in this paper. Since J_φ and J_θ are different in each point of the edge such as $\mathbf{V}_x$ shown in Fig. 2(b), non-unique vectors are resulted from conversion of a current vector $\mathbf{V}$ from Cartesian to spherical coordinates.

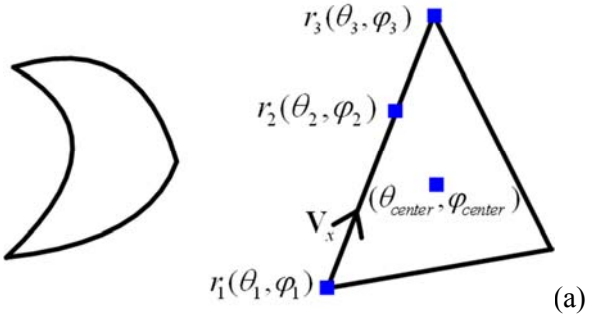

Fig. 2. (a) Curvilinear triangle, (b) Linear triangle.

The drawback stated above can be greatly reduced by employing the centers of the field and source triangles in spherical coordinates. Since there are unique transformations of vectors from spherical to Cartesian coordinates, conversion of a spherical dyad to a Cartesian dyad can be exactly implemented. As an example the conversion

equation of $\hat{r}\hat{r}$ component of a spherical dyad is extracted as follows:

$$\hat{r}\hat{r} = (\sin\theta_f \cos\varphi_f \, \hat{x} + \sin\theta_f \sin\varphi_f \, \hat{y} + \cos\theta_f \, \hat{z}) \quad (4)$$
$$(\sin\theta_s \cos\varphi_s \, \hat{x} + \sin\theta_s \sin\varphi_s \, \hat{y} + \cos\theta_s \, \hat{z}),$$

in which subscripts *f* and *s* refer to field and source points, respectively. Accordingly each spherical DGFs ($\overline{\mathbf{G}}_1^{(fs)}$) can be converted to Cartesian DGFs ($\overline{\mathbf{G}}_2^{(fs)}$). Relations between Cartesian and spherical components are presented in appendix 2. The electric field vector can be expressed as:

$$\mathbf{E}^{(Cartesian)} = -j\omega\mu_f \iint_{s'} \overline{\mathbf{G}}^{(Cartesian)} . \mathbf{J}^{(Cartesian)}(\mathbf{r}')\, ds'. \quad (5)$$

Using this approach is efficient when a vector is requested as the output of an antenna problem solution. Therefore, all E_x, E_y, E_z components of electric field can be calculated to determine near and far field radiation patterns of an antenna. Far-field components can be calculated by integrating over the multiplication of the current of each source element and its corresponding DGFs and using the superposition principle. The 20 first terms in the summation of $\overline{\mathbf{G}}_E^{(11)}$ and $\overline{\mathbf{G}}_E^{(12)}$ are used to calculate electric fields due to $\mathbf{J}_{s1}$ and $\mathbf{J}_{s2}$, respectively. It should be mentioned that the algebraic conversion of nine spherical dyads to Cartesian ones requires very low time and memory (about 0.001 times the memory and time taken by calculation of 20 spherical harmonics terms for such an antenna structure). It takes about 9 minutes to compute E- or H-planes radiation patterns (with 60 divisions of θ) with a Core 2 Quad @ 2.86 GHz processor. The proposed method has more calculation speed in comparison with the CAD simulator packages and can be utilized in analysis of various spherical antennas such as a probe fed spherical microstrip antenna with radial current components.

III. RESULTS

In order to validate the proposed method, a prototype of an aperture-coupled antenna with a parasitic element is fabricated and tested. A 3mm*20mm slot is cut on a 5cm radius PEC sphere and is excited at its center through a 20cm RG-58U coaxial cable of 50Ω characteristic impedance. A circular patch has been made from a RT/duroid 5870 substrate of 0.8mm thickness and with a relative permittivity of 2.33 located above the slot. Due to the thin substrate, the whole dielectric over PEC sphere can be modeled by a partial dielectric under patch antenna. A circular parasitic element is located above the patch by using a spacer material of unit relative permittivity. The implemented aperture-coupled antenna is shown in Fig. 3.

(a)

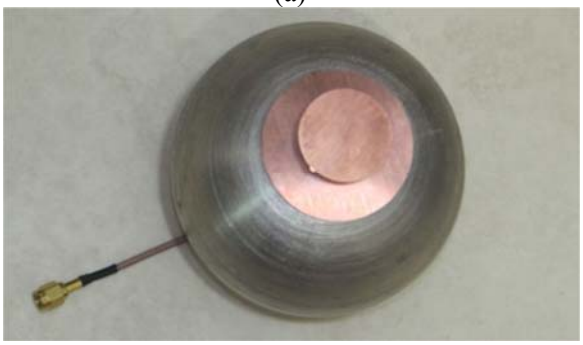

(b)

Fig. 3. Prototype of the spherical aperture-coupled antenna; (a) slotted PEC shell, (b) patch antenna with parasitic element.

The conformal patch antenna has been divided into 100 triangles yielding 140 common edges and the parasitic element has been divided into 36 triangles leading to 48 common edges. Figure 4 demonstrates the input impedance obtained from analytical solution and the measurement of the antenna. The E- and H-planes radiation patterns of the antenna are measured at 3.1GHz and are shown in Fig. 5. As it can be noticed, directed patterns with low side lobes levels are achieved from this antenna. Good agreement between the results of the proposed method and measurement is obtained. An efficiency of 87% at 3.1GHz has been obtained which is measured by Bluetest reverberation chamber. Figure 6 illustrates the antenna gain with and without the parasitic element. An increase in antenna gain is notable with the presence of the parasitic element. As

shown in Fig. 7, parasitic element makes antenna radiation patterns more directive but it increases cross polarization radiations. The latter is because of electromagnetic fields perturbation due to the existence of parasitic element.

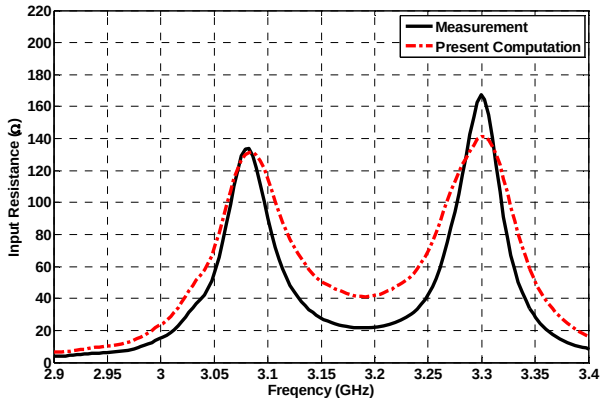

(a)

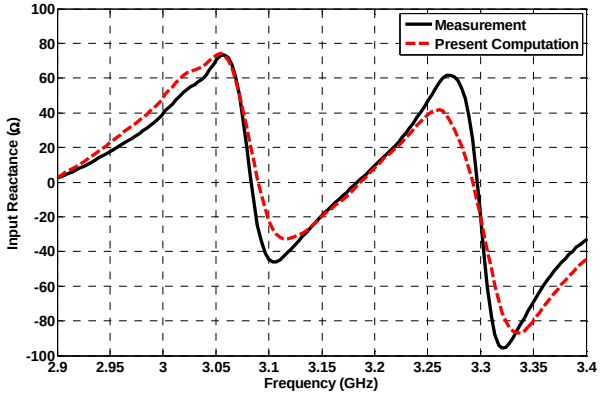

(b)

Fig. 4. Input impedance of the proposed antenna; (a) Resistance, (b) Reactance.

IV. CONCLUSION

In this paper, an efficient full-wave method has been presented to analyze spherical aperture-coupled patch antenna with parasitic element. Spatial domain DGFs in conjunction with MoM have been used in the analysis. Coupling effects between the patches and the slot have been investigated. In this method, electromagnetic fields vectors at entire medium have been computed by meshing the antenna into linear triangles in Cartesian coordinates and converting equations of dyads from spherical to Cartesian coordinates. Robustness and accuracy of the proposed method have been validated by comparing the results obtained from the proposed method with those of the measurement. Directive radiation patterns and low side lobes levels are some specific features of this antenna. The effect of the parasitic element on radiation patterns and gain of the antenna has been shown. An improvement is achieved in antenna gain and directivity due to the existence of the parasitic element.

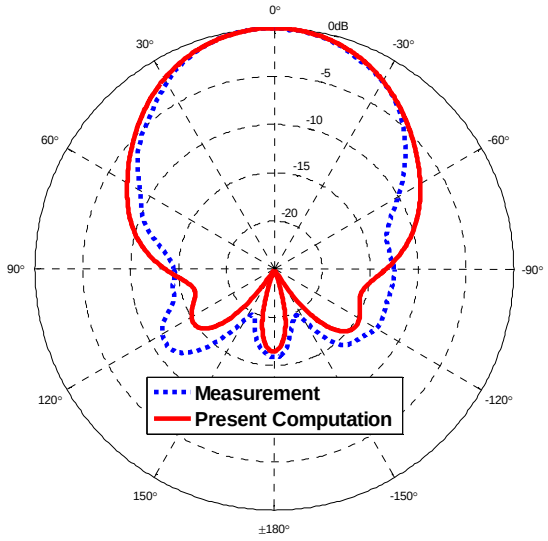

(a)

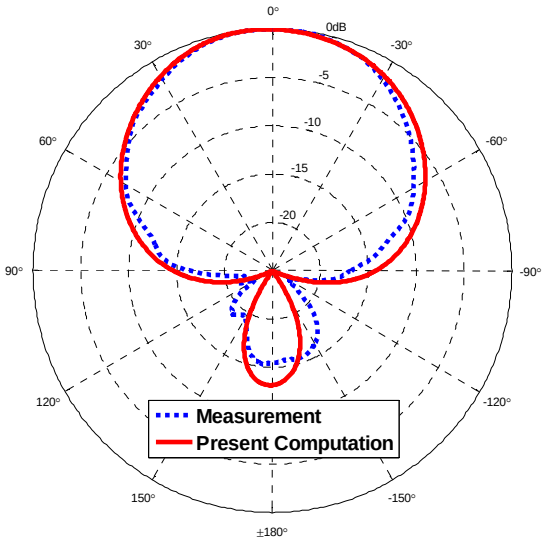

(b)

Fig. 5. Radiation patterns of the aperture-coupled antenna with parasitic element; (a) E-Plane, (b) H-Plane.

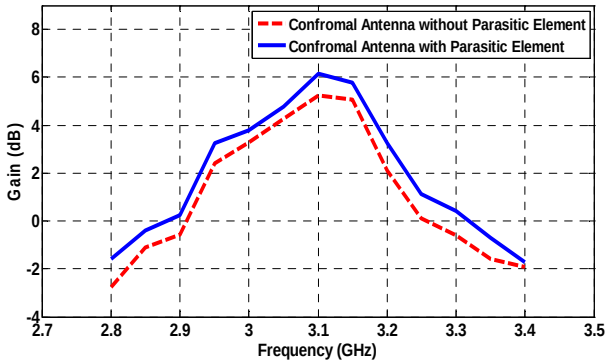

Fig. 6. Gain of the aperture-coupled antenna with and without parasitic element.

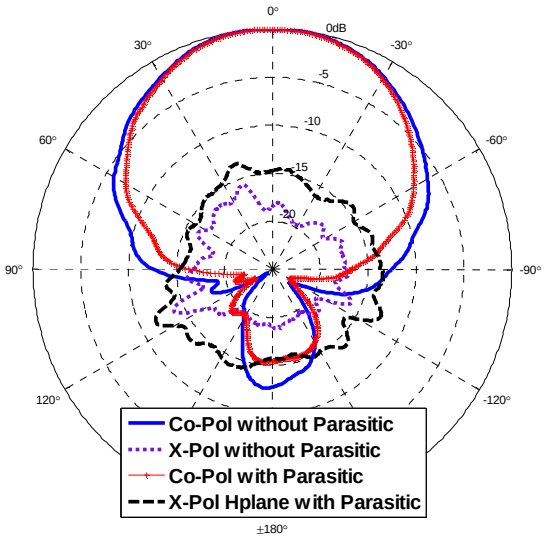

(a)

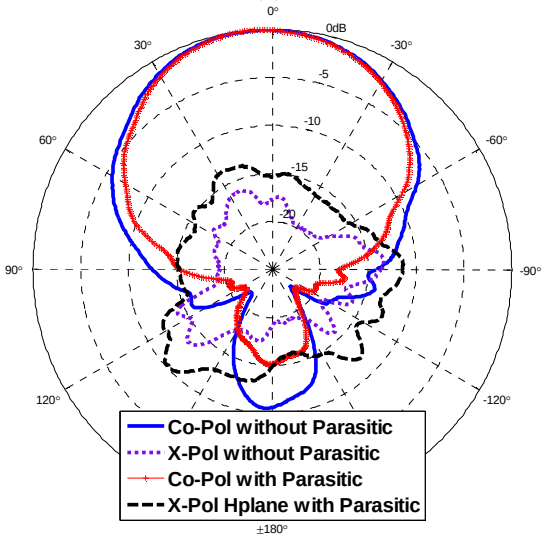

(b)

Fig. 7. Co- and cross-polar radiation (H-plane); (a) f=3.1GHz, (b) f=3.2GHz.

V. APPENDIX1

Magnetic DGFs ($\overline{\mathbf{G}}_M$) can be computed by using $\overline{\mathbf{G}}_E$ in [18] and the duality theorem. For the present antenna (Fig. 1), the scattering components of magnetic field in conformal radiating elements (layers 1, 2) due to the slot (layer 3) can be obtained by using the magnetic current source in layer *s=3* and considering the centers of triangles conformed in layers *f=1,2* as field points.

$$\overline{\mathbf{G}}_M^{(13)} = \frac{jk_3}{4\pi}\sum_{n=0}^{\infty}\sum_{m=0}^{n}\left(2-\delta_m^0\right)\frac{2n+1}{n(n+1)}\frac{(n-m)!}{(n+m)!} \times \begin{Bmatrix} a_M^{13}\mathbf{M}^{(2)}_{\substack{e\\o}mn}(k_f)\,\mathbf{M}'_{\substack{e\\o}mn}(k_3) \\ +b_M^{13}\mathbf{M}^{(2)}_{\substack{e\\o}mn}(k_f)\,\mathbf{M}'^{(2)}_{\substack{e\\o}mn}(k_3) \\ +a_N^{13}\mathbf{N}^{(2)}_{\substack{e\\o}mn}(k_f)\,\mathbf{N}'_{\substack{e\\o}mn}(k_3) \\ +b_N^{13}\mathbf{N}^{(2)}_{\substack{e\\o}mn}(k_f)\,\mathbf{N}'^{(2)}_{\substack{e\\o}mn}(k_3) \end{Bmatrix}, \tag{A1}$$

$$\overline{\mathbf{G}}_M^{(23)} = \frac{jk_3}{4\pi}\sum_{n=0}^{\infty}\sum_{m=0}^{n}\left(2-\delta_m^0\right)\frac{2n+1}{n(n+1)}\frac{(n-m)!}{(n+m)!} \times \begin{Bmatrix} a_M^{23}\mathbf{M}^{(2)}_{\substack{e\\o}mn}(k_f)\,\mathbf{M}'_{\substack{e\\o}mn}(k_3) \\ +b_M^{23}\mathbf{M}^{(2)}_{\substack{e\\o}mn}(k_f)\,\mathbf{M}'^{(2)}_{\substack{e\\o}mn}(k_3) \\ +a_N^{23}\mathbf{N}^{(2)}_{\substack{e\\o}mn}(k_f)\,\mathbf{N}'_{\substack{e\\o}mn}(k_3) \\ +b_N^{23}\mathbf{N}^{(2)}_{\substack{e\\o}mn}(k_f)\,\mathbf{N}'^{(2)}_{\substack{e\\o}mn}(k_3) \\ +c_M^{23}\mathbf{M}_{\substack{e\\o}mn}(k_f)\,\mathbf{M}'_{\substack{e\\o}mn}(k_3) \\ +d_M^{23}\mathbf{M}_{\substack{e\\o}mn}(k_f)\,\mathbf{M}'^{(2)}_{\substack{e\\o}mn}(k_3) \\ +c_N^{23}\mathbf{N}_{\substack{e\\o}mn}(k_f)\,\mathbf{N}'_{\substack{e\\o}mn}(k_3) \\ +d_N^{23}\mathbf{N}_{\substack{e\\o}mn}(k_f)\,\mathbf{N}'^{(2)}_{\substack{e\\o}mn}(k_3) \end{Bmatrix}, \tag{A2}$$

where δ_m^0 is the Kronecker delta, k_i is the propagation constant in i-th layer **M**, **N** and are orthogonal Eigen vectors in spherical coordinates with properties explained in [7]. The spherical Bessel or Hankel functions are of the second kind. Dyadic coefficients ($a_{M,N}$, $b_{M,N}$, $c_{M,N}$, $d_{M,N}$) can be computed by using the duality theorem.

VI. APPENDIX2

The components of the transformed spherical DGFs ($\overline{\mathbf{G}}_1^{(fs)}$) to Cartesian DGFs ($\overline{\mathbf{G}}_2^{(fs)}$) are expressed as follow:

$$\bar{\mathbf{G}}_1^{(fs)}=\begin{pmatrix} G_{rr} & G_{r\theta} & G_{r\varphi} \\ G_{\theta r} & G_{\theta\theta} & G_{\theta\varphi} \\ G_{\varphi r} & G_{\varphi\theta} & G_{\varphi\varphi} \end{pmatrix} \Rightarrow \bar{\mathbf{G}}_2^{(fs)}=\begin{pmatrix} G_{xx} & G_{xy} & G_{xz} \\ G_{yx} & G_{yy} & G_{yz} \\ G_{zx} & G_{zy} & G_{zz} \end{pmatrix} \quad \text{(A3)}$$

$$\begin{aligned} G_{xx} &= G_{rr}\sin\theta_f\cos\varphi_f\sin\theta_s\cos\varphi_s \\ &+G_{r\theta}\sin\theta_f\cos\varphi_f\cos\theta_s\cos\varphi_s - G_{r\varphi}\sin\theta_f\cos\varphi_f\sin\varphi_s \\ &+G_{\theta r}\cos\theta_f\cos\varphi_f\sin\theta_s\cos\varphi_s - G_{\varphi r}\sin\varphi_f\sin\theta_s\cos\varphi_s \\ &+G_{\theta\theta}\cos\theta_f\cos\varphi_f\cos\theta_s\cos\varphi_s - G_{\theta\varphi}\cos\theta_f\cos\varphi_f\sin\varphi_s \\ &-G_{\varphi\theta}\sin\varphi_f\cos\theta_s\cos\varphi_s + G_{\varphi\varphi}\sin\varphi_f\sin\varphi_s \end{aligned} \quad \text{(A4)}$$

$$\begin{aligned} G_{xy} &= G_{rr}\sin\theta_f\cos\varphi_f\sin\theta_s\sin\varphi_s \\ &+G_{r\theta}\sin\theta_f\cos\varphi_f\cos\theta_s\sin\varphi_s + G_{r\varphi}\sin\theta_f\cos\varphi_f\cos\varphi_s \\ &+G_{\theta r}\cos\theta_f\cos\varphi_f\sin\theta_s\sin\varphi_s - G_{\varphi r}\sin\varphi_f\sin\theta_s\sin\varphi_s \\ &+G_{\theta\theta}\cos\theta_f\cos\varphi_f\cos\theta_s\sin\varphi_s + G_{\theta\varphi}\cos\theta_f\cos\varphi_f\cos\varphi_s \\ &-G_{\varphi\theta}\sin\varphi_f\cos\theta_s\sin\varphi_s - G_{\varphi\varphi}\sin\varphi_f\cos\varphi_s \end{aligned} \quad \text{(A5)}$$

$$\begin{aligned} G_{xz} &= G_{rr}\sin\theta_f\cos\varphi_f\cos\theta_s - G_{r\theta}\sin\theta_f\cos\varphi_f\sin\theta_s \\ &+G_{\theta r}\cos\theta_f\cos\varphi_f\cos\theta_s - G_{\varphi r}\sin\varphi_f\cos\theta_s \\ &-G_{\theta\theta}\cos\theta_f\cos\varphi_f\sin\theta_s + G_{\varphi\theta}\sin\varphi_f\sin\theta_s \end{aligned} \quad \text{(A6)}$$

$$\begin{aligned} G_{yx} &= G_{rr}\sin\theta_f\sin\varphi_f\sin\theta_s\cos\varphi_s \\ &+G_{r\theta}\sin\theta_f\sin\varphi_f\cos\theta_s\cos\varphi_s - G_{r\varphi}\sin\theta_f\sin\varphi_f\sin\varphi_s \\ &+G_{\theta r}\cos\theta_f\sin\varphi_f\sin\theta_s\cos\varphi_s + G_{\varphi r}\cos\varphi_f\sin\theta_s\cos\varphi_s \\ &+G_{\theta\theta}\cos\theta_f\sin\varphi_f\cos\theta_s\cos\varphi_s - G_{\theta\varphi}\cos\theta_f\sin\varphi_f\sin\varphi_s \\ &+G_{\varphi\theta}\cos\varphi_f\cos\theta_s\cos\varphi_s - G_{\varphi\varphi}\cos\varphi_f\sin\varphi_s \end{aligned} \quad \text{(A7)}$$

$$\begin{aligned} G_{yy} &= G_{rr}\sin\theta_f\sin\varphi_f\sin\theta_s\sin\varphi_s \\ &+G_{r\theta}\sin\theta_f\sin\varphi_f\cos\theta_s\sin\varphi_s + G_{r\varphi}\sin\theta_f\sin\varphi_f\cos\varphi_s \\ &+G_{\theta r}\cos\theta_f\sin\varphi_f\sin\theta_s\sin\varphi_s + G_{\varphi r}\cos\varphi_f\sin\theta_s\sin\varphi_s \\ &+G_{\theta\theta}\cos\theta_f\sin\varphi_f\cos\theta_s\sin\varphi_s + G_{\theta\varphi}\cos\theta_f\sin\varphi_f\cos\varphi_s \\ &+G_{\varphi\theta}\cos\varphi_f\cos\theta_s\sin\varphi_s + G_{\varphi\varphi}\cos\varphi_f\cos\varphi_s \end{aligned} \quad \text{(A8)}$$

$$\begin{aligned} G_{yz} &= G_{rr}\sin\theta_f\sin\varphi_f\cos\theta_s - G_{r\theta}\sin\theta_f\sin\varphi_f\sin\theta_s \\ &+G_{\theta r}\cos\theta_f\sin\varphi_f\cos\theta_s + G_{\varphi r}\cos\varphi_f\cos\theta_s \\ &-G_{\theta\theta}\cos\theta_f\sin\varphi_f\sin\theta_s - G_{\varphi\theta}\cos\varphi_f\sin\theta_s \end{aligned} \quad \text{(A9)}$$

$$\begin{aligned} G_{zx} &= G_{rr}\cos\theta_f\sin\theta_s\cos\varphi_s - G_{r\varphi}\cos\theta_f\sin\varphi_s \\ &+G_{r\theta}\cos\theta_f\cos\theta_s\cos\varphi_s - G_{\theta r}\sin\theta_f\sin\theta_s\cos\varphi_s \\ &-G_{\theta\theta}\sin\theta_f\cos\theta_s\cos\varphi_s + G_{\theta\varphi}\sin\theta_f\sin\varphi_s \end{aligned} \quad \text{(A10)}$$

$$\begin{aligned} G_{zy} &= G_{rr}\cos\theta_f\sin\theta_s\sin\varphi_s + G_{r\varphi}\cos\theta_f\cos\varphi_s \\ &+G_{r\theta}\cos\theta_f\cos\theta_s\sin\varphi_s - G_{\theta r}\sin\theta_f\sin\theta_s\sin\varphi_s \\ &-G_{\theta\theta}\sin\theta_f\cos\theta_s\sin\varphi_s - G_{\theta\varphi}\sin\theta_f\cos\varphi_s \end{aligned} \quad \text{(A11)}$$

$$\begin{aligned} G_{zz} &= G_{rr}\cos\theta_f\cos\theta_s - G_{r\theta}\cos\theta_f\sin\theta_s \\ &-G_{\theta r}\sin\theta_f\cos\theta_s + G_{\theta\theta}\sin\theta_f\sin\theta_s \end{aligned} \quad \text{(A12)}$$

ACKNOWLEDGMENT

The authors would like to thank the Research Institute of ICT (former Iran Telecommunication Research Center) for its support.

REFERENCES

[1] D. M. Pozar, "Microstrip Antenna Aperture-Coupled to a Microstrip-Line," *Electron. Lett*., vol. 21, no. 2, pp.49-50, Jan. 1985.

[2] W. Huang and A. Kishk, "Apertures-Coupled Multi-Layer Cylindrical Dielectric Resonator Antennas and Modal Analysis," 23rd Annual Review of Progress in *Applied Computational Electromagnetics Society (ACES) Journal*, Verona, Italy, pp. 1117-1120, March 2007.

[3] J. G. Davis, P. Shakespeare, and N. Kiley, "Evaluation of Circular Aperture Transmission Coefficients in the Presence of Obscurations," *Applied Computational Electromagnetics Society (ACES) Journal*, vol. 26, no. 9, pp. 723-728, Sep. 2011.

[4] K. W. Leung, W. C. Wong, K. M. Luk, and E. K. N. Yung, "Circular Polarized Dielectric Resonator Antenna Excited by Dual Conformal Strips," *Electron. Lett.*, vol. 36, no. 6, pp. 484-486, March 2000.

[5] K. W. Leung and H. K. Ng, "Theory and Experiment of Circularly Polarized Dielectric Resonator Antenna with a Parasitic Patch," *IEEE Trans. Antennas Propag.*, vol. 51, no. 3, pp. 405-412, March 2003.

[6] W. C. Chew, *Waves and Fields in Inhomogeneous Media*, IEEE Press Series on Electromagnetic Waves, New York, 1995.

[7] C. T. Tai, *Dyadic Green's Functions in Electromagnetics Theory*, IEEE Press Series on Electromagnetic Waves, New York, 1994.

[8] J. V. Bladel, *Electromagnetic Fields*, second edition, IEEE press, John Wiley & Sons, Inc., 2007.

[9] T. V. B. Giang, M. Thiel, and A. Dreher, "A Unified Approach to the Analysis of Radial Waveguides, Dielectric Resonators, and Microstrip Antennas on Spherical Multilayer Structures," *IEEE Trans. Microwave Theory and Techniques* , vol. 53, no. 1, pp. 404-409, Jan. 2005.

[10] K. W. Leung, K. M. Luk, K. Y. A. Lai, and D. Lin, "Theory and Experiment of a Coaxial Probe Fed Hemispherical Dielectric Resonator Antenna," *IEEE Trans. Antennas Propag.,* vol. 41, no. 10, pp. 1390-1398, Oct. 1993.

[11] K. W. Leung and H. K. Ng, "The Slot-Coupled Hemispherical Dielectric Resonator Antenna with a Parasitic Patch: Applications to the Circularly Polarized Antenna and Wide-Band Antenna," *IEEE Trans. Antennas Propag.,* vol. 53, no. 5, pp. 1762-1769, May 2005.

[12] K. K. So and K. W. Leung, "Bandwidth Enhancement and Frequency Tuning of the Dielectric Resonator Antenna using a Parasitic Slot in the Ground Plane," *IEEE Trans. Antennas Propag.,* vol. 53, no. 5, pp. 1762-1769, May 2005.

[13] J. Sun and T. Li, "Dual-Frequency Dielectric Resonator Antenna with Inverse T-shape Parasitic Strip," 23rd Annual Review of Progress in *Applied Computational Electromagnetics Society (ACES) Journal,* Honolulu, Hawaii, April 2005.

[14] J. S. Meiguni, M. Kamyab, and A. Hosseinbeig, "Electromagnetic Characteristics of Conformal Dipole Antennas over a PEC Sphere," *Progress In Electromagnetics Research M*, vol. 26, pp. 85-100, 2012.

[15] K. W. Leung, "Theory and Experiment of a Rectangular Slot on a Sphere," *IEEE Trans. Microwave Theory Tech.,* vol. MTT-46, no. 12, pp. 2117-2123, Dec. 1998.

[16] S. M. Rao, D. R. Wilton, and A. W. Glisson, "Electromagnetic Scattering by Surfaces of Arbitrary Shape," *IEEE Trans. Antennas Propag.*, vol. 30, pp. 409-418, May 1982.

[17] R. F. Harrington, *Time-Harmonic Electromagnetic Fields*, IEEE press, John Wiley & Sons Inc., 2001.

[18] L.W. Li, P. S. Kooi, M. S. Leong, and T. S. Yeo, "Electromagnetic Dyadic Green's Function in Spherically Multilayered Media," *IEEE Trans. Microwave Theory Tech.,* vol. 42, pp. 2302-2310, Dec. 1994.

Javad Soleiman Meiguni was born in 1982 in Tehran, Iran. He received his B.S. from Semnan University, Semnan, Iran and M.S. from K. N. Toosi University of Technology, Tehran, Iran in 2005 and 2008, respectively all in Electrical Engineering. He has been working towards Ph.D. in Telecommunications at K. N. Toosi University of Technology, Tehran, Iran. He has participated in many projects inside and outside the university. Currently, he is working on analysis and design of spherical aperture-coupled antennas using Dyadic Green's Functions. His research is mainly focused on the areas of antennas and EM modeling, numerical techniques in electromagnetics, antenna design and measurement, active and passive microwave and millimeter-wave circuit design.

Manoochehr Kamyab received the B.S. and M.S. from the University of Tehran, Tehran, Iran, and the PhD degree from Michigan State University, in 1982, in Electrical Engineering. His research interests include the metamaterials and their applications in antenna engineering, electrically small antennas, microwave and millimeter-wave circuits, and mobile communication systems. He is currently a professor in the Department of Electrical Engineering, K.N. Toosi University of Technology, Tehran, Iran. Professor Kamyab is leading a group of graduate students in the areas of negative-refraction metamaterials and their microwave applications, integrated antennas and components for broad-band wireless telecommunications, novel antenna beam-steering techniques, millimeter and sub-millimeter-wave circuits, as well as scattering and inverse scattering problems.

Ahmad Hosseinbeig was born in 1983 in Tehran, Iran. He received the B.S. in Electrical Engineering from Shahid Bahonar University, Kerman, Iran and M.S. in Telecommunications Engineering from K. N. Toosi University of Technology, Tehran, Iran in 2006 and 2008, respectively. He is presently studying for a Ph.D. in Telecommunications Engineering at K. N. Toosi University of Technology, Tehran, Iran. He is currently working on analysis and design of spherical aperture-coupled Dielectric Resonator Antennas (DRA) using Dyadic Green's Functions. His main research interests are in the fields of numerical techniques in electromagnetic theory, antenna design and measurement, microwave and high frequency circuit design.